CHINESE JOURNAL OF MECHANICAL ENGINEERING
Vol. 26, No. 2, 2013

DOI: 10.3901/CJME.2013.02.414, available online at www.springerlink.com; www.cjmenet.com; www.cjmenet.com.cn

Scale Effects on Propeller Cavitating Hydrodynamic and Hydroacoustic Performances with Non-uniform Inflow

YANG Qiongfang[1,*], WANG Yongsheng[1], and ZHANG Zhihong[2]

1 *College of Marine Power Engineering, Naval University of Engineering, Wuhan 430033, China*
2 *College of Science, Naval University of Engineering, Wuhan 430033, China*

Received April 19, 2012; revised December 20, 2012; accepted December 26, 2012

Abstract: Considering the lack of theoretical models and ingredients necessary to explain the scaling of the results of propeller cavitation inception and cavitating hydroacoustics from model tests to full scale currently, and the insufficient reflection of the nuclei effects on cavitation in the numerical methods, the cavitating hydrodynamics and cavitation low frequency noise spectrum of three geometrically similar 7-bladed highly skewed propellers with non-uniform inflow are addressed. In this process, a numerical bridge from the multiphase viscous simulation of propeller cavitation hydrodynamics to its hydro-acoustics is built, and the scale effects on performances and the applicability of exist scaling law are analyzed. The effects of non-condensable gas(NCG) on cavitation inception are involved explicitly in the improved Sauer's cavitation model, and the cavity volume acceleration related to its characteristic length is used to produce the noise spectrum. Results show that, with the same cavitation number, the cavity extension on propeller blades increases with diameter associated with an earlier shift of the beginning point of thrust decline induced by cavitation, while the three decline slopes of thrust breakdown curves are found to be nearly the same. The power of the scaling law based on local Reynolds number around 0.9R section is determined as 0.11. As for the smallest propeller, the predominant tonal noise is located at blade passing frequency(BPF), whereas 2BPF for the middle and both 2BPF and 3BPF for the largest, which shows the cavitating line spectrum is fully related to the interaction between non-uniform inflow and fluctuated cavity volume. The predicted spectrum level exceedance from the middle to the large propeller is 6.65 dB at BPF and 5.94 dB at 2BPF. Since it just differs less than 2 dB to the increment obtained by empirical scaling law, it is inferred that the scale effects on them are acceptable with a sufficient model scale, and so do the scaling law. The numerical implementation of cavitating hydrodynamics and hydro-acoustics prediction of propeller in big scale in wake has been completed.

Key words: propeller, cavitation inception, cavitation noise, scale effect, cavitation model, turbulence model

1 Introduction

As demonstrated experimentally to the cavitation of 3-D hydrofoil and submerged body by KELLER[1], obvious scale effects including velocity scale and size scale effect on cavitation inception and cavitation developing level were presented. As for the marine propeller, SZANTYR[2] further addressed the scale effects in detail through cavitation experiments. According to that, the tip vortex inception cavitation number differed significantly between the model with fully scale due to the differences in static pressure distribution, in water quality (non-condensable gas content(NCG)), in boundary layer separation and in velocity and geometry scale. And the propeller cavitation extent was also different even with a same cavitation index. To demonstrate the practical worthiness of the medium size cavitation testing facilities in predicting the acoustic characteristics of a propeller and to provide useful noise data in full-scale using the scaling law recommended by the 18th ITTC Cavitation Committee, ATLAR, et al[3], presented cavitation tunnel tests of a model propeller and the comparison between the extrapolated results to its full-scale measurements. It was shown that a useful basis for the propeller noise prediction in full-scale could be provided by the extrapolation procedure mentioned with about 6 dB to 18 dB discrepancies in 1 kHz frequency band. Referring to the scaling law, the increment of the spectrum level from model to full-scale is related exponentially to the geometry scale, tip circumferential velocity, cavitation index, fluid density and reference distance for which the noise is predicted. As a practical application, SHEN, et al[4], concluded that the exponent value of 0.28 represented the Reynolds number effect on propeller cavitation noise at the critical point with 20 dB below the maximum noise level for both the full-scale and model scale, through trial noise measurements of the full-scale noise level of USS 212 class submarine and its model with a scale ratio of 14.5. Under

* Corresponding author. E-mail: yqfhaijun2008@126.com
This project is supported by National Natural Science Foundation of China(Grant No. 51009144)

this circumstance, the background noise had negligible effect on cavitation noise due to the well-developing cavitation. Additionally, if the cavitation inception speed (CIS) at model scale pointed to the silent critical point on the S curve of noise, i.e. 0 dB above the background noise, the exponent 0.315 would be used to predict the CIS of full-scale, and the scale effects could be involved reasonably. It means the exponent 0.315 is related to the effect of Reynolds number on well-developed cavitation of propeller.

In the framework of single phase viscous simulation to the scaling of tip vortex cavitation inception noise of hydrofoil and ship propeller, HSIAO, et al[5–6], PARK, et al[7] had proposed integrated technical solutions in the recent past. Exactly, in conjunction with the Reynolds-averaged Navier-Stokes(RANS) computations for single-phase flow field, the spherical or non-spherical micro-bubble dynamics model with or without accounting for the nuclei size distribution was used to detect the cavitation inception with a visual or an acoustic criterion. Due to the unawareness of the pre-defined threshold, it is difficult to apply this method directly to the propeller cavitation inception and cavitating hydro-acoustics prediction at full-scale until now, then there is little prospect that the scale effects on them could be clearly clarified. According to SINGHAL, et al[8] and GINDROZ, et al[9], both volume fraction and mass fraction of NCG and the turbulent pressure fluctuation will affect the cavitation inception significantly. Likewise, even the free-stream turbulence is one of the main factors contributing to the scale effects on the inception of cavitation, which has been found by KORKUT, et al[10] this year. Consequently, adding these effects explicitly into the process of cavitation turbulent flow simulation is supposed to be more reasonable than the single way solution with nuclei effect involved as a supplement. It is just the original calling to the cavitation multiphase simulation for cavitating noise prediction.

However, benefiting from the fast and convenient realization of the potential flow theory, the inviscid surface panel method based on velocity has been widely used in propeller sheet cavitation simulation and its radiated noise evaluation in the recent years, including SALVATORE, et al[11], EKINCI, et al[12], SEOL, et al[13]. Following the realization, the single pulsing spherical bubble radiated noise theory is mostly used to compute the noise spectrum of cavitating monopole source, like HU[14] and ZHANG[15]. From another perspective, SEOL, et al[13] and TESTA[16] both used a more robust mathematical model, i.e. the Ffowcs Williams and Hawkings integral equation to predict the propeller cavitation noise. Although the predicted sound pressure level at blade passing frequency(BPF) and its harmonics were found to be good agreement with that of experiment results, the NCG effects are still hard to be carried into the process of numerical simulation.

Currently, many researchers' attention has turned back to cavitation multiphase simulation for higher accuracy with the prospect of developing better cavitation model or depending on model calibration. Since all the multiphase flow model, turbulent model, cavitation model and phase change threshold pressure acting as a whole to affect the cavitation simulation, no optimal composite models acing as a universal solution to cavitating hydrodynamics in marine engineering have been brought up along with integrated validation until now. Due to the popularization of commercial CFD solvers, the mixture multi-phase modeling method develops relatively fast and acceptably, and several cavitation models based on homogeneous multi-phase transport equations have proved to be extremely valuable for marine propeller cavitation flow recently, like SINGHAL's model[8], SAUER's model[17], KUNZ's model[18], and ZWART's model[19]. Among these models, RHEE, et al[20] used the SINGHAL full model embedded in FLUENT 6.1 code to simulate MP 017 propeller sheet cavitation and predict its thrust breakdown performance, LINDAU, et al[21] used KUNZ'S model involved in UNCLE-M software for the cavity pattern simulation and cavitation breakdown performance maps prediction of the NSRDC 4381 and INSEAN E779A propellers, and added an axial-flow waterjet. Pointing to the same propeller P4381, KIM[22] chose the Sauer model within the open source code OpenFOAM to verify its simulated cavity extension, and a higher accuracy was shown at last. Additionally, for analyzing and comparing different numerical cavitation models to serve as a complement to experiments for waterjet pump cavitating flow, OLSSON[23] investigated the SINGHAL, KUNZ and SAUER's model combined with $k-\varepsilon$ RNG turbulent model with turbulent viscosity modification by density function on sheet cavitation of hydrofoil and pump. It was shown that, as for the rotary cavitating flow, the Sauer model was most efficient for global force prediction and the cavitation break-off point determination. Furthermore, MORGUT, et al[24] assessed the three mass transfer models, i.e. SINGHAL, KUNZ and ZWART activated in ANSYS CFX 12 commercial code on E779A propeller's cavity patterns and global force validation. It was clarified that the two equation SST turbulence model could guarantee the same level of accuracy as the computationally more expensive BSL-RSM turbulence model. And the computational results obtained from the particular condition, using alternatively the different well-tuned mass transfer models, were very close to each other. In addition, JI, et al[25], also chose the default ZWART cavitation model and SST turbulence model in CFX code to investigate the pressure fluctuation induced by cavitating propeller with non-uniform inflow. The amplitudes of first three harmonics of BPF were acceptably predicted with a maximum difference reaching to 20%. From these reviews, it is concluded that, with reasonable physical models including both cavitation model and turbulence model, adding a good meshing strategy and an efficient and robust CFD solver, CFX for instance, reliable numerical cavitating

flow can be represented and visualized.

More recently, accounting for the effects of both mass fraction and volume fraction of the NCG on cavitation inception at the same time, YANG, et al[26–28] introduced an improved SAUER's cavitation model associated with a modified SST turbulent model by Compiling Expression Language(CEL) in CFX 12 solver to investigate the propeller cavitating turbulent flow and cavitation inception phenomena. Using these models, the effects of both NCG and turbulence on cavitation inception and cavitating bubble growth were considered by the equations of mixture density and phase-changing threshold pressure. Since the pressure distribution was the decisive factor for cavitation inception in numerical simulation, a rule that when the cavitation index reaches to its critical number, the pressure coefficient distribution around a certain blade section, i.e. at the radius of 0.9*R*, is unaltered has been drawn to determine the propeller cavitation inception time. This numerical process is just contrary to that in cavitation tunnel tests with pressure reduction. The physical gas content is modeled by constants of NCG mass fraction and volume fraction. The critical point of cavitation inception is that, as increasing cavitation number, the pressure coefficient around the given section is nearly superposed to the result in single-phase non-cavitation simulation. Then, the visual or acoustic criteria of cavitation inception can be achieved by the relative changing amplitude of the separate L2 norms of pressure coefficient acting as a similar manner to verification and validation of a point variable. As a result, the inception buckets were predicted satisfactorily for both no-skewed and highly skewed propellers by multiphase flow CFD calculation method initially. On this basis, in order to investigate the effects of thrust loads and cavity extension on the discrete line spectrum frequency and its spectrum source level, a method coupling the multi-phase flow cavitation simulation with pulsating spherical bubble radiated noise theory has been undertaken to predict both the 5- and 7-balded propellers' cavitating noise spectrum by YANG, et al[29]. A numerical system to measure the cavitating hydrodynamics and noise performances of the ship propellers has been constructed there.

Continuing to demonstrate the viability and importance of this method for propeller performances assessment in big scale, and describe the scale effects on cavitating breakdown performances, cavitation inception and radiated tonal noise at low frequency, three geometrically similar 7-bladed highly skewed propellers of different scales and of the same non-dimensional incoming wake flow are addressed in this research. According to the numerical results, the applicability of the empirical scaling law will be analyzed to give deep insights into cavitation noise prediction for propeller in full-scale.

In the following, the numerical models employed are presented firstly in section 2, and followed by their calibration and validation in section 3, including cavitation model, turbulence model and cavitating noise mathematical model. Then the scale effects on cavitating hydrodynamics and hydro-acoustics of three propellers are provided in section 4. At the end, our concluding remarks are given.

2 Numerical Models

2.1 Cavitation model and turbulence model

According to Refs. [26–28], the mixture multi-phase flow model including both the NCG mass and volume fraction in mixture density is used again. Both the effects of nuclei distribution and dissolved air content on cavitation inception can be considered explicitly in that way. At this moment, the total number of mixture phase is n=3, which is more reasonable than the reviewed literatures with two phases. Since the velocity slip between the main phase and secondary phase is rather small for high Reynolds number and small vapor bubbles, the assumption for no velocity slip is still used as the same as that in Refs. [19–25]. On a volume fraction basis, the mixture density is expressed as

$$\rho_{\mathrm{m}} = [\alpha_{\mathrm{v}}\rho_{\mathrm{v}} + (1-\alpha_{\mathrm{v}}-\alpha_{\mathrm{g}})\rho_{\mathrm{l}}]/(1-f_{\mathrm{g}}), \tag{1}$$

where α_{v} and ρ_{v} are vapor volume fraction and its density respectively, α_{g} and f_{g} are volume and mass fraction of NCG respectively, ρ_{l} is the water density. The mass transferred through cavitation is modeled by the transport equation for the vapor mass fraction:

$$f_i \equiv \alpha_i \frac{\rho_i}{\rho_{\mathrm{m}}} (i = 1,\ 2,\ \cdots,\ n), \tag{2}$$

in which subscript i stands for the ith phase. And the transport equation for the vapor is

$$\frac{\partial}{\partial t}(\rho_{\mathrm{m}} f_{\mathrm{v}}) + \nabla \bullet (\rho_{\mathrm{m}} \boldsymbol{v}_{\mathrm{m}} f_{\mathrm{v}}) = A, \tag{3}$$

where f_{v} is vapour mass fraction, $\boldsymbol{v}_{\mathrm{m}}$ is the mixture velocity. A is the mass transfer source between water and vapour, which is usually divided into two items $A = \dot{m}^{+} + \dot{m}^{-}$, $\dot{m}^{+}$ and $\dot{m}^{-}$ stand for vapor vaporization (bubble growth) and condensation (bubble collapse) process respectively. The improved Sauer cavitation model is presented here again. Its mass transfer rates are written as

$$\begin{cases} \dot{m}^{+} = \dfrac{C_{\mathrm{p}} 3\alpha_{\mathrm{g}}(1-\alpha_{\mathrm{v}})\rho_{\mathrm{v}}}{R_{\mathrm{B}}} \sqrt{\dfrac{2}{3}\dfrac{|p_{\mathrm{v}} - p|}{\rho_{\mathrm{l}}}}\, \mathrm{sgn}(p_{\mathrm{v}} - p), \\ \dot{m}^{-} = \dfrac{C_{\mathrm{d}} 3\alpha_{\mathrm{v}}\rho_{\mathrm{v}}}{R_{\mathrm{B}}} \sqrt{\dfrac{2}{3}\dfrac{|p_{\mathrm{v}} - p|}{\rho_{\mathrm{l}}}}\, \mathrm{sgn}(p_{\mathrm{v}} - p), \end{cases} \tag{4}$$

where empirical coefficients are $C_{\mathrm{p}} = 50$ and $C_{\mathrm{d}} = 0.01$. The phase-change threshold pressure p_{v} is modeled by

$$p_{\mathrm{v}} = p_{\mathrm{sat}} + \frac{1}{2}(0.39\rho_{\mathrm{m}} k), \tag{5}$$

in which k is turbulent kinetic energy, p_{sat} is the saturation vapor pressure with 3 540 Pa. With calculative experiences, optimum NCG mass fraction and volume fraction are $f_g = 1\times10^{-6}$ and $\alpha_g = 7.8\times10^{-4}$ respectively, and the bubble initial average radius is $R_B = 1.5$ μm. Explicitly, an earlier cavitation inception is represented by the combination of mixture density and the turbulence fluctuation. And the NCG effects are included directly by this formulation. Similar to Eq. (5), a further slight modification is adopted as

$$p_v = p_{sat} + 0.39\rho_m k(1-\alpha_v) \tag{6}$$

to apply the pressure turbulence term only in vapor phase presence so to speed up the solution convergence. Since the calculated vapor volume fraction with iso-surface $\alpha_v = 0.5$ to limit the propeller sheet cavity extension seems reasonable in reviewed Refs. [21–22, 24] except JI, et al[25] and KIM[22] with $\alpha_v = 0.1$, the two modifications are the same under that occasion. Actually, the appropriate iso-surface boundary depends on the initial cavitation inception time according to the comprehensive validation of cavity area of E779A propeller in Ref. [26]. If the modified phase-change threshold pressure is used, the cavitation inception is earlier than that being controlled by the constant vapor pressure of what had been used by JI, et al and KIM, so to produce more vapor volume fraction under steady numerical tests, and a larger iso-surface boundary is needed subsequently.

Comparing to the Sauer model, its differences are as follows:

(1) Introducing the NCG volume fraction to vapor vaporization term and replacing the density ratio ρ_l/ρ_m as constant coefficient C.

(2) Expressing the radius of bubbles in denominator as a function of vapor volume fraction α_v and replacing the number of bubbles per unit volume n_0 to the initial constant $R_B = 1.5$ μm.

(3) Determining the initial vapor volume fraction α_{v0} by the initial number of bubbles given.

The improvements made by the author mainly locate at involving the NCG mass and volume fractions in mixture density at the same time and determining their reasonable values after a large number of tests on cavitating flows of NACA 66 (mod) hydrofoil and propeller NSRDC 4381 in Refs. [30–31]. Following Eqs. (1), (2), (4), (5), the f_g directly influences the ρ_m, and then to both turbulent viscosity μ_t and p_v, so that the cavitation inception point is affected. At the same time, α_g directly drives the evaporation rates $\dot{m}^+$ to change, and then to change the cavity extension.

To solve the turbulent cavitating flow, the SST model with modified wall function is implemented to provide turbulence closure in this research to overcome the singularity at separation points where the near wall velocity approaches zero, so that they can be applied to any fine mesh element. And a further calibration of the turbulent viscosity is introduced as

$$\mu_t = \rho_m k/\omega \tag{7}$$

referring to Refs. [20, 32]. In the equation, ω is turbulent vortex frequency. The physical interpretation of this calibration is in respect of the numerical calculation. Specifically, with a local refinement grid topology, Eq. (7) will enlarge the application scope of low Reynolds number equation to some extent, so to perform better the applicability of ω transport equation to model separate flow with curvature change and the un-sensitivity of the ε equation to free stream vortex frequency.

2.2 Cavitating noise mathematical model

According to tunnel tests in model scale, propeller cavitation are mainly divided into three types: tip vortex cavitation, blade surface cavitation, and hub vortex cavitation. Of the various types of cavitation, because of the vortex cavitation remaining in negative pressure regions for relatively longer time and collapsing with less fluctuated energy, the suction side sheet cavitation produces the highest noise level, and hub vortex cavitation the least[33]. In other words, the sheet cavitation on suction side is the main noise source of a cavitating propeller.

In the field of time-domain acoustic analogy for noise prediction, both the propeller blade thickness rotation and unsteady sheet cavity volume fluctuation can be simplified as monopole sources, while the blade surface pressure fluctuation called loading noise is equivalent to the dipole source term and the stochastic noise with broadband characteristics is modeled as a quadrupole source term. Applying this method, SEOL, et al[34], had proved numerically that the thickness noise component of propeller was negligible comparing to the unsteady loading noise especially under the non-uniform inflow condition. Due to the internal low Mach number, the fluctuated volume radiating noise component will dominate the propeller's far-field noise intensity once the cavitation occurs. It means, precisely tracking the cavity volume periodic fluctuation is essential to determine the main noise source of a cavitating propeller.

As an application of the Ffowcs Williams-Hawkings equation integral method, Farassat 1A formulation in time-domain can predict noise from an arbitrary shaped object in motion without the numerical differentiation of the observer time[35]. When the turbulent quadrupole noise source is neglected, the sound pressure at observer (x, t) is the sum of thickness noise p_T' and loading noise p_L' contributions of all source nodes on the object. It is expressed as

$$p'(\boldsymbol{x},t) = p'_T(\boldsymbol{x},t) + p'_L(\boldsymbol{x},t), \tag{8}$$

where the thickness noise component is obtained by

introducing the sound Green's function in unbounded field[36],

$$p'_{\mathrm{T}}=\int_S G\frac{1-\boldsymbol{M}_\infty\bullet\boldsymbol{D}}{1-\boldsymbol{M}_{\mathrm{s}}\bullet\boldsymbol{D}}\left(\rho\dot{v}_n+\gamma\rho v_n\frac{\dot{\boldsymbol{M}}_{\mathrm{s}}\bullet\boldsymbol{R}+\boldsymbol{M}_{\mathrm{s}}\bullet\dot{\boldsymbol{R}}}{1-\boldsymbol{M}_{\mathrm{s}}\bullet\boldsymbol{D}}\right)\mathrm{d}S-c\int_S G\frac{\rho v_n}{R'}(\boldsymbol{M}_\infty\bullet\boldsymbol{R}-\boldsymbol{M}_{\mathrm{s}}\bullet\boldsymbol{R}(1-\boldsymbol{M}_\infty\bullet\boldsymbol{D}))\mathrm{d}S, \tag{9}$$

in which the first term in right accounts for the near-field while the second for far-field, and the Green's function is read as

$$G=\frac{\gamma}{4\pi R'(1-\boldsymbol{M}_{\mathrm{s}}\bullet\boldsymbol{D})}, \tag{10}$$

in which R' is the distance from source to observer, inflow Mach number $\boldsymbol{M}_\infty=\boldsymbol{V}_s/c$, $\boldsymbol{V}_s$ is inflow speed, $\gamma^2=\dfrac{1}{1-\left|\boldsymbol{M}_\infty\right|^2}$, the source Mach number relative to fixed reference frame is $\boldsymbol{M}_{\mathrm{s}}=\dfrac{\partial\boldsymbol{y}}{\partial\tau}/c$, the radiation vector is equal to $\boldsymbol{D}=\gamma\boldsymbol{R}-\gamma^2\boldsymbol{M}_\infty$, $\boldsymbol{R}=(\boldsymbol{r}+\gamma^2(\boldsymbol{M}_\infty\bullet\boldsymbol{r})\boldsymbol{M}_\infty)/R'$, observer-source distance $\boldsymbol{r}=\boldsymbol{x}-\boldsymbol{y}$, $\boldsymbol{l}=p\boldsymbol{n}$ is the force extracted from pressure, v_n is the surface normal velocity. Variable τ means the integration at retarded time.

The calculations of retarded time τ for any point on the blade and its normal velocity v_n are crucial to the p'_{T}. Once the sheet cavitation occurs, the normal velocity of partial acoustic nodes shifts from blade surface to the cavity surface. With a zero thickness hypothesis of the cavity in panel surface method, extracting the cavity normal velocity is the same as that of non-cavitation. While in the viscous CFD simulation, since the sheet cavity extension is visualized by iso-surface of the vapor volume fraction mapped on CFD mesh elements, wherein the fluid variables are extrapolated from the centered nodes rather then the element surfaces in generic CFD solvers, hence, the predicted cavity surface is not closely coincident with the blade surface even with extremely small first height nodes. At this moment, the discrepancy between the acoustic source nodes information output from CFD solver in every transient time-step with the mesh element on blades will be a barrier into the hydro-acoustic tool. This problem is being actively sought in author's team now.

From another point of view, the pulsating spherical noise source radiating noise is given by

$$p'(r)=\frac{\rho_{\mathrm{l}}}{4\pi r}\frac{\mathrm{d}^2V_{\mathrm{c}}}{\mathrm{d}t^2}, \tag{11}$$

where V_{c} is the cavity volume. If the whole blades' cavity extension is equivalent to a spherical source with the same volume, the far-field radiated noise at any point can be obtained by this equation. Neither by the surface panel method nor the viscous CFD calculation, the periodic-fluctuated sheet cavity area versus rotating angles can be integrated directly in post-process of the results. When the spherical hypothesis is used, the cavity volume can be easily obtained to predict its the sound pressure. Refs. [14–15] just used this simplification in conjunction with the surface panel method to calculate propeller cavitation noise. However, the cavities on propeller blades are far from being spherical according to the experiments in PEREIAR, et al[37–38]. The vapor extension (cavity area) generated by unsteady sheet cavitation of both hydrofoil and propeller can be represented by a characteristic length l_{c}, and the cavity volume V_{c} is proportional to l_{c}. Their specific expressions are written as

$$l_{\mathrm{c}}=\sqrt{E_{\mathrm{c}}},\quad \frac{\mathrm{d}^2V_{\mathrm{c}}}{\mathrm{d}t^2}=\left[6l_{\mathrm{c}}(\mathrm{d}l_{\mathrm{c}}/\mathrm{d}t)^2+3l_{\mathrm{c}}^2(\mathrm{d}^2l_{\mathrm{c}}/\mathrm{d}t^2)\right]. \tag{12}$$

As a result, aims at predicting propeller cavitating noise, the fluctuated cavity area is captured by viscous CFD runs firstly, and then the second derivative of the cavity volume is obtained by Eq. (12) to deduce the sound pressure using Eq. (11). It is supposed to be more reasonable than the spherical cavity assumption in the view of flow patterns.

3 Validation of the Cavitation Simulation

With a block-structured and flow-adaptive grid topology, Fig. 1 shows the surface mesh of propeller E779A and its simulated cavity patterns at advance ratio J=0.77 and cavity areas under lightly, moderately and heavily cavitation level conditions by the improved Sauer model and modified SST model above. The cavitation index σ based on inflow speed and the rotating speed cavitation index σ_n are introduced into the numerical calculation to control the pressure p_{out} on the outlet surface of numerical domain after activating the cavitation model, which are defined as

$$\sigma=\frac{p_{\mathrm{out}}-p_{\mathrm{v}}}{0.5\rho_{\mathrm{l}}v_{\mathrm{s}}^2},\quad \sigma_n=\frac{p_{\mathrm{out}}-p_{\mathrm{v}}}{0.5\rho_{\mathrm{l}}(nD)^2}, \tag{13}$$

where v_{s} is incoming flow velocity, n and D are propeller rotating speed and diameter respectively. As σ_n decreases, the boundary pressure changes to represent the pressure-decreasing in cavitation tests. In the figure, A_{c} is the cavity area and note that A_0 is the blade face area for $r/R\geqslant 0.3$ with respect to the experiment[39]. Under moderately cavitation level condition ($0.1\leqslant A_{\mathrm{c}}/A_0<0.25$), the simulated cavity area is very close to the experiment, wherein a little small for the lightly cavitation level ($A_{\mathrm{c}}/A_0<0.1$) due to the wall roughness effect and bigger than the measurement for heavily condition ($0.25\leqslant A_{\mathrm{c}}/A_0<0.5$) because of the bubble cavitation area being included. The numerical domain and boundary

conditions of this test are shown in Fig. 2. Uniform incoming velocity and averaged static pressure are located on inlet and outlet respectively. The second-order upwind scheme is used for the convection term and high resolution option for turbulence numeric accuracy in the solving of governing equations.

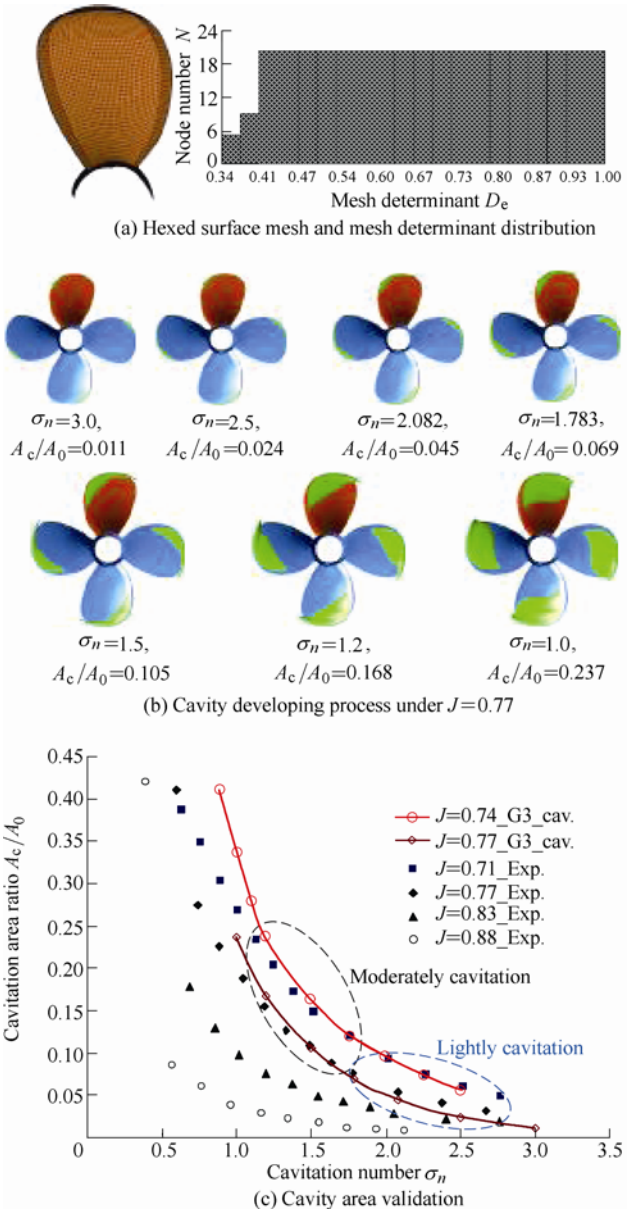

Fig. 1. Validation of the propeller sheet cavitation

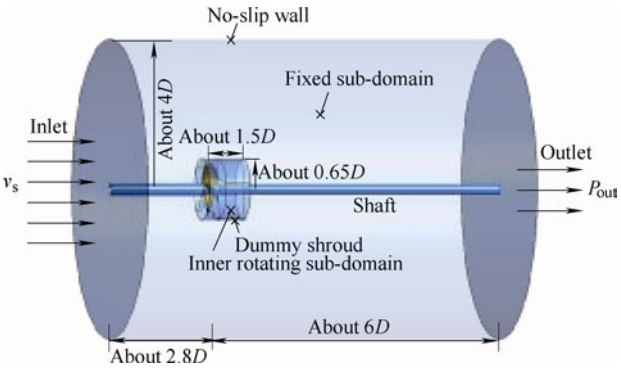

Fig. 2. Numerical domain and boundary conditions

Using the inception rule "when $\sigma > \sigma_i$, the pressure coefficients distribution of blade tip section is relatively unaltered", the predicted visual tip vortex cavitation inception number is proved to be an excellent agreement with the experiment, which can be seen in Ref. [26] in detail. From the qualitative and quantitative comparison, it is seen that, with the aid of proper refinement grid topology around the blade surface, the adopted cavitation model combined with the modified turbulence model are extremely valuable for sheet cavitation simulation under the level of moderately cavitation, and also be able to capture well the beginning point of cavitation inception and developing area of cavitation.

4 Scale Effects Analysis

4.1 Scale effects on cavitation hydrodynamics

In the following, all the simulations are undertaken on three similar 7-bladed propellers with diameter 250 mm, 500 mm and 1 000 mm respectively. For simplicity they are named as small, middle and big propeller. Their single passage numerical domains and corresponding hexed structure meshes are all completed by procedural realizations presented in Ref. [40]. Note that, the mesh nodes density on leading edge region, trailing edge region, tip section area and blades surface are all local-refined gradually with diameter increase. The surface mesh details are seen in Fig. 3. In order to minimize the effects of mesh quality differences, the mesh minimum determinant indexes of three propellers are all above 0.2 associated with close mesh density and average Yplus distribution on blade surfaces. The total number of mesh nodes in three single passage domains is controlled with a grid refinement ratio $r_G = 1.7$. For decreasing the numerical errors induced by variables interpolation between periodic interfaces with un-matching mesh nodes, the full-passage numerical domains of three propellers are included in the calculations. The numerical domain and boundary conditions in non-cavitation single-phase RANS calculation are the same as that in Fig. 2. Fig. 4 shows the calculated open water characteristics of three propellers. This figure also shows the results of the model tests for the small propeller. The agreement is seen to excellent good again. Under the same advance ratio, the thrust coefficient K_t increases but torque coefficient K_q decreases with larger Reynolds number of bigger geometry scale. So the derived open water efficiency increases obviously with diameter associated with a smaller increase rate further away the design point. In the figure, the variables are defined as

$$J = \frac{v_s}{nD},\quad K_t = \frac{T}{\rho n^2 D^4},\quad K_q = \frac{Q}{\rho n^2 D^5},\quad \eta_0 = \frac{J_0}{2\pi}\frac{K_t}{K_q}, \tag{14}$$

where T and Q are axial thrust and break torque respectively. Subscript 0 stands for the uniform inflow condition, and subscripts s, m and b stand for the small, middle and big respectively. The rotating speeds of three propellers are set as $n_s = 20$ r/s, $n_m = 15$ r/s, $n_b = 10$ r/s to match the tunnel tests. So the Reynolds number Re_n based on rotating speed and diameter differs by an order of magnitude between the small and big propeller, which can be enlarged subsequently to full-scale analysis.

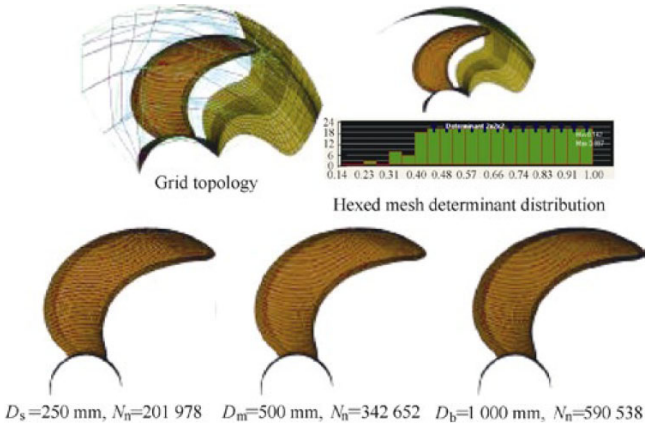

Fig. 3. Grid topology, mesh determinant and surface mesh details of all scaled propellers

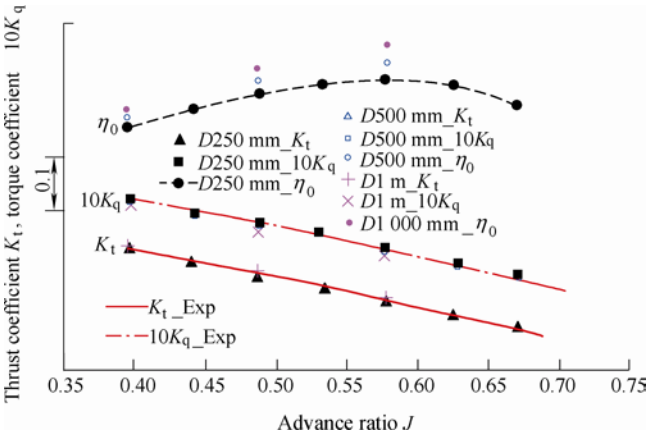

Fig. 4. Predicted open water characteristics of propellers

In order to decrease the differences caused by the interactions between non-uniform inflow with blade leading edge of different scaled propeller, the same non-dimensional nominal wake of full-appended SUBOFF submarine is used as the incoming flow. Its introducing method is as follows. Firstly, the nominal wake information including both geometry coordinates and three velocity components are extracted as a profile on propeller disk plane with a radius of $1.1D_s$, then the variables are transferred and smoothed by conservative extrapolation to the same area region on inlet boundary surface of the small propeller. Outer this region, the uniform flow still exists. It means the affected radial region by boundary layer flow of submarine appendages is limited. As regarding to the middle and big propellers, the transformation of incoming flow profiles are divided into two steps. Firstly the geometry coordinates are scaled with scale ratio to the larger inlet boundary surface with a same relative area. Then three velocity components are multiplied with a ratio corresponding to the same advance ratio to insure the close loadings on three propellers. Besides, the left regions on the inlet surfaces of these two propellers are still set as uniform inflow boundary conditions, and their incoming velocities are determined by the examined advance ratio.

Fig. 5 shows three propellers' propulsion performance curves with nominal wake. The same scale effects reflected on larger K_t and smaller K_q due to bigger geometry scale under the same advance ratio are presented again. So does the derived propulsive efficiency as that with uniform inflow. If we predict the big propeller's propulsion performance directly from the small one, the maximum and minimum discrepancy of K_t will reach 3.5% and 2.9% respectively within the region of J=0.209–0.403, and the error bounds of K_q will be 3.2% to 3.8% at the same time. That is, the correction needed for the global force variables is smaller than that with uniform inflow to serve the engineering directly during the initial phase of design.

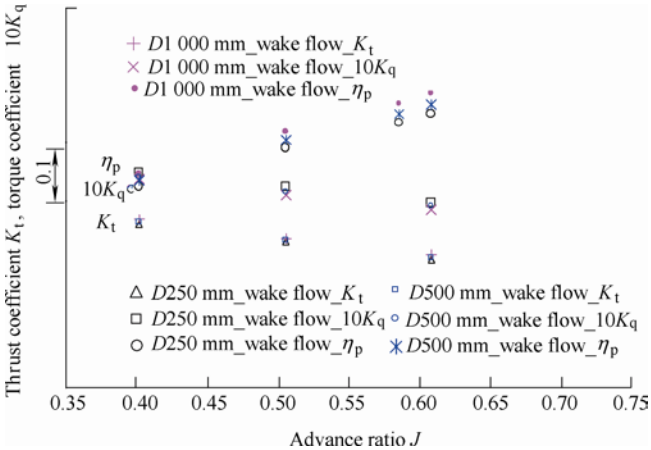

Fig. 5. Propulsive performances of propellers with the same non-dimensional incoming wake flow

In order to extract the pulsating cavity area information, the numerical propeller cavitation tests are conducted by changing p_{out} to influence σ. The improved Sauer cavitation model is activated from the initial simulated non-cavitation flow results with non-uniform inflow. Fig. 6

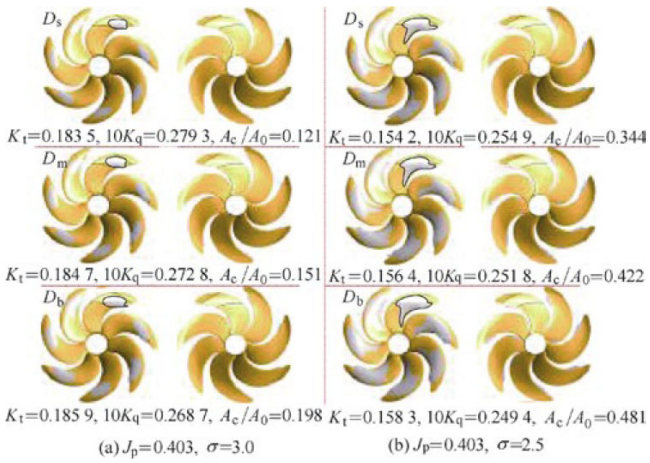

Fig. 6. Comparison of cavitation patterns of propellers with non-uniform inflow

shows the cavitation patterns of three propellers under the same advance ratio and cavitation number. It is obviously that the cavity area ratio increases with geometry scale associated with a bigger K_t and a smaller K_q. In these plots, A_0 is the area of propeller disk plane, and the cavities are all visualized by iso-surface of $\alpha_v = 0.5$. Under a given advance ratio, the propeller thrust and torque breakdown curves can be predicted by decreasing gradually the cavitation index number. Fig. 7 and Fig. 8 just present the three propellers' cavitation breakdown performances and their corresponding cavity area ratios versus cavitation indexes. The calculated thrust, torque and cavity area under uniform inflow condition are also given in these two figures.

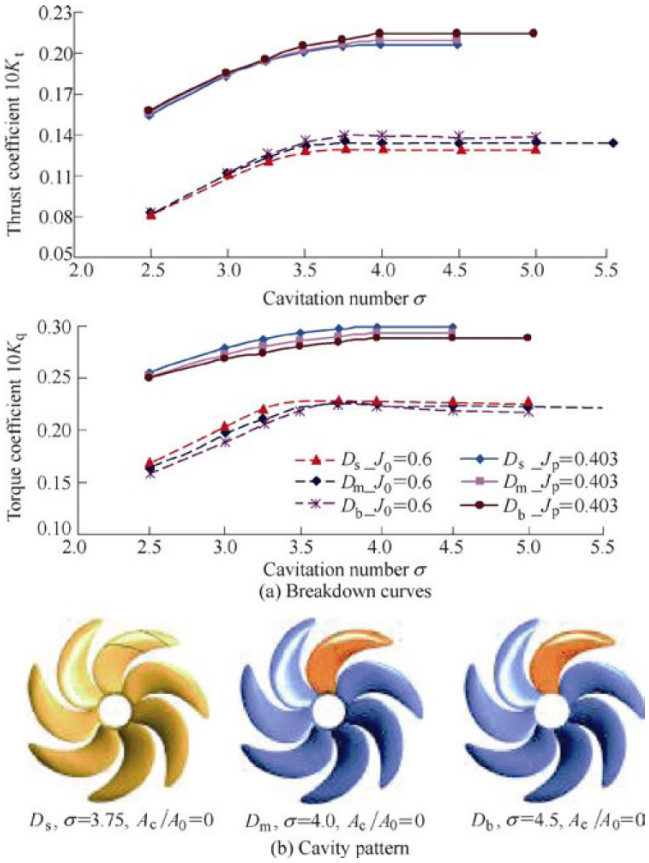

Fig. 7. Thrust and torque breakdown performances of propellers with uniform and non-uniform inflow

As demonstrated in Fig. 7, the beginning point of thrust decline induced by cavitation is moved forwards with the increase of propeller diameter. Under this occasion, the three cavitation indexes are 3.75, 4.0 and 4.5 respectively with respect to three critical points with no visual back surface cavitation. Relating to the same phenomena, these three points are located at $\sigma = 3.5$, 3.75 and 4.0 respectively under uniform inflow condition. It means the effects of non-uniform inflow on the critical point of thrust decline are tightly related to the inflow itself, and comparable earlier effect is presented for a given inflow-propeller combination. In addition, the three slope indexes of thrust decline curves are almost the same, which can be also related to the reason of comparable effects of interactions between incoming flow with blades. Following that, the effects of developing cavitation on global force variables will be a major factor analyzed in the following.

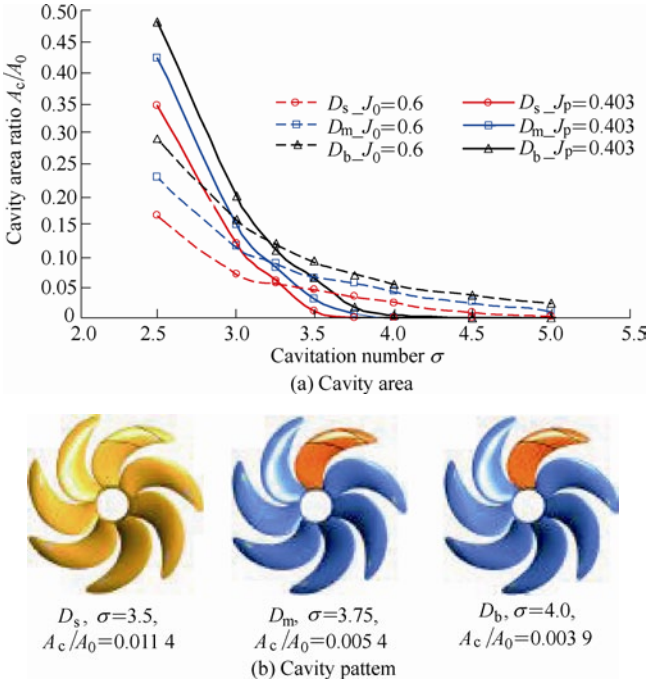

Fig. 8. Cavity area ratio versus cavitation numbers of propellers

As depicted in Fig. 8, the cavitation developing rates under non-uniform inflow condition are significantly faster than that with uniform inflow. When the local tip vortex on back face occurs for the three propeller, their corresponding cavitation numbers are $\sigma = 3.5$, 3.75 and 4.0 respectively. Under this condition, the cavity extension of big propeller is the smallest, and its location of cavity moves up along the span compared to the other two propellers. With respect to the three inflection points, three propellers are just under tiny cavitation level with about 1% of the cavity area ratio.

Fig. 9 shows the pressure coefficient distribution around $0.9R$ blade section of three propellers with non-uniform inflow. Applying the inception rule, the tip vortex inception cavitation numbers $\sigma_i = 4.0$, 4.5 and 5.0 are obtained for three propellers. Obviously, the inception time is much earlier than the beginning time of thrust decline, which is consistent with the conclusion of that of propeller NSRDC 4381 in Ref. [27], seen in Fig. 10.

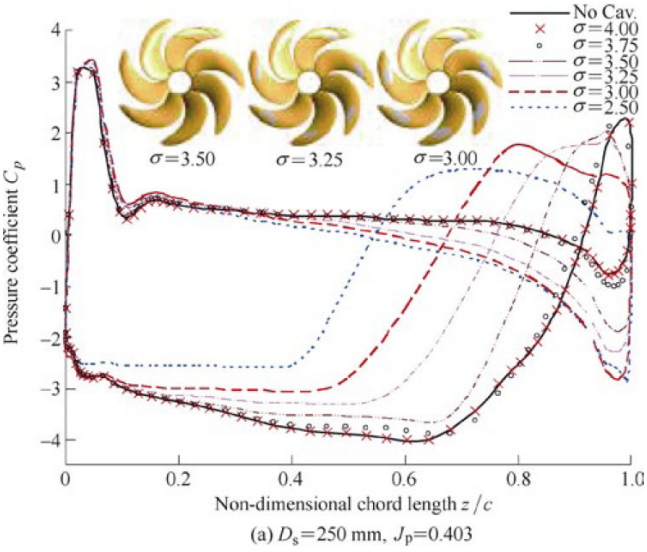

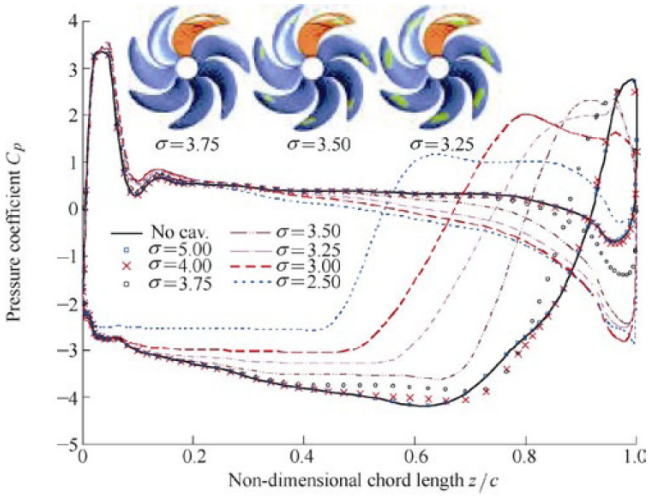

(b) D_m=500 mm, J_p=0.403

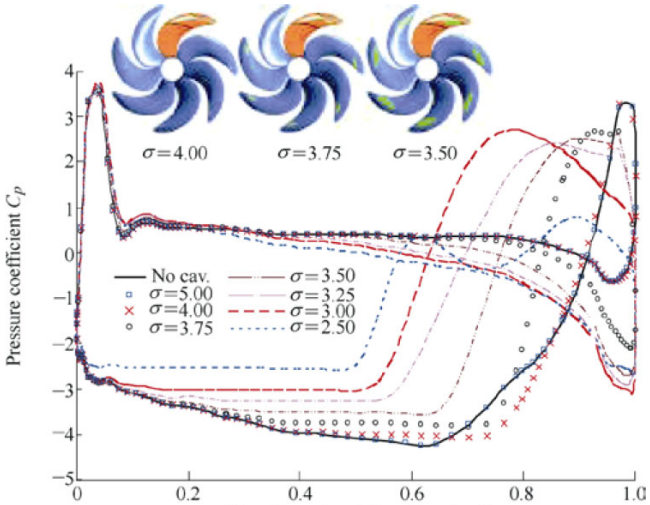

(c) D_b=1 000 mm, J_p=0.403

Fig. 9. Pressure coefficient distribution around 0.9R section of propellers with non-uniform inflow

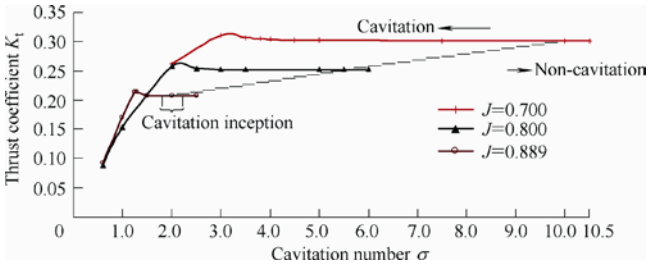

Fig. 10. Thrust breakdown performances of 4381 propeller

Following the predicted inception number, if the effect on cavitation inception number is related to the Reynolds number, the cavitation index σ_n based on rotating speed can be deduced from σ. Exactly, the initial indexes based on rotating speed are $\sigma_{ni}=1.44$, 1.62 and 1.8 respectively for the three propellers. When the local Reynolds number based on the total velocity and chord of 0.9R section is introduced, the flow parameters of all scales are shown in Table 1. The local Reynolds number is defined as

$$Re_{0.9R}=v_{0.9R}\bullet c_{0.9R}/\nu=\sqrt{v_a^2+(0.9\pi nD)^2}\bullet c_{0.9R}/\nu, \tag{15}$$

where $c_{0.9R}$ is chord of 0.9R section, ν is viscosity, v_a is the axial velocity component. If the classical power law relationship between the Reynolds number and cavitation inception number is used,

$$\sigma_{ni}\propto Re^{\gamma}, \tag{16}$$

the power value of γ equals to 0.11, which is smaller than the value of 0.22 calculated by HSIAO, at al[5]. However, it is in a satisfactory accordance with the power 0.12 found numerically in Ref. [41] for a highly-skewed 5-bladed propeller.

Table 1. Comparison of parameters of three propellers

Parameter	Small	Middle	Big
Diameter D / mm	250	500	1000
Rotating speed n / (r • s^{-1})	20	15	10
Inflow speed v_a / (m • s^{-1})	2.016	3.024	4.032
Chord $C_{0.9R}$ / mm	694.8	1389.6	2779.2
Reynolds number $Re_{0.9R}$	9.85×10^6	2.96×10^7	7.88×10^7
Reynolds number Re_n	1.24×10^6	3.72×10^6	9.93×10^6
Inception number σ_i	4.0	4.5	5.0
Inception number σ_{ni}	1.44	1.62	1.8

4.2 Scale effects on cavitating hydroacoustics

As mentioned in section 2.2, the periodic-pulsating cavity area or the cavity volume determines the low frequency cavitating noise spectrum, including its tonal components and spectrum level. The time-dependent signal can be obtained by cavitation transient simulation. In numerical tests, the iterative time-step of three propellers are set as $\Delta t_s=2.78\times10^{-4}$ s, $\Delta t_m=3.7\times10^{-4}$ s and $\Delta t_b=5.56\times10^{-4}$ s respectively, which are all associated with 2 degrees of blade rotation. According to the sampling theorem, their relating effective maximum frequencies are 1 800 Hz, 1 350 Hz and 900 Hz. After running for five cycles, all the flow variables extracted for analysis are output from the fifth revolution.

Fig. 11 shows cavity area fluctuation versus azimuth angles under the condition of $J_p=0.403, \sigma=2.5$ for three propellers, their fluctuation in frequency domain with non-dimensional frequency $St=f/n$ are also shown in this figure. It seems that two peaks are appeared in the time domain both for the middle and big propeller. Regarding to the frequency domain, only the axial passing frequency (APF) and BPF tonal components exist for small propeller, while both BPF and 2BPF line spectrum dominate the middle propeller's signal. Excepting for the BPF and 2BPF components, the BPF harmonics stretching to 5 are still obvious for the big propeller. Besides, the fluctuating amplitude of cavity area increases significantly with the geometry scale.

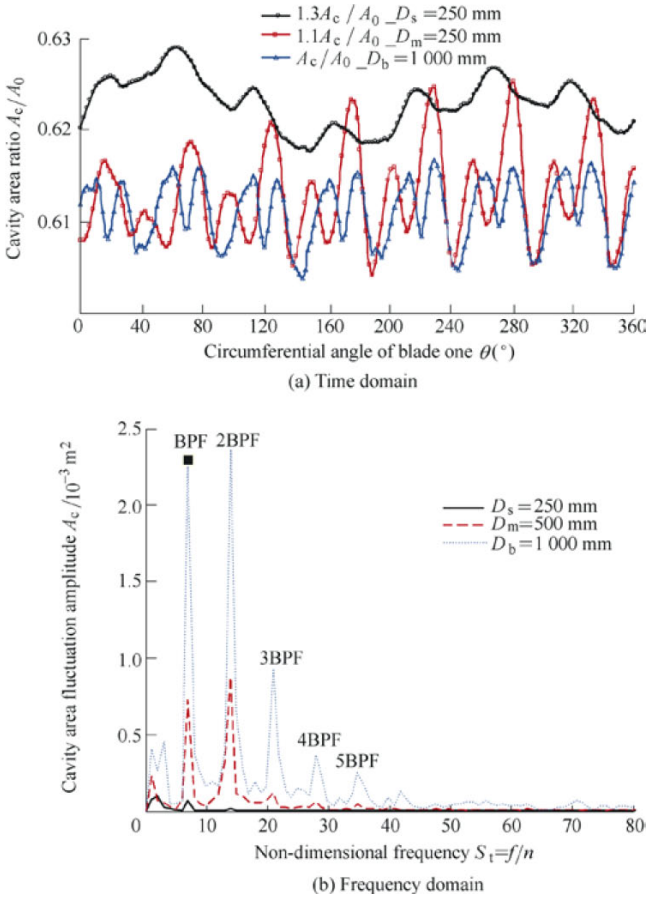

Fig. 11. Cavity area fluctuation under $J_p = 0.403, \sigma = 2.5$

After the acceleration of cavity volume is obtained, the cavitating low frequency noise spectrum can be plotted by substituting its second derivative into Eq. (11). Fig. 12 shows the calculated noise of all scales under non-uniform inflow condition. The noise spectrum predicted by spherical cavity hypothesis are also shown in it for comparison. The source-observer distance of small, middle and big propeller is $r_s = 1$ m, $r_m = 2$ m, and $r_b = 4$ m corresponding to the same relative distance. It is found that the sound pressure calculated by spherical cavity is bigger than that by the cavitation characteristic length for all the scales. Exactly, the amplitude exceedance at the pre-dominated BPF frequency is 3.22 dB, 2.55 dB and 2.17 dB for the small, middle and big propeller respectively. It means the predicted difference between these two approaches increases inversely with the geometry scale. Using the cavitation characteristic length, the predicted cavitating spectrum level at BPF frequency is 153.92 dB, 173.15 dB and 179.81 dB re. 1 μPa and 1 Hz for the three propellers. At the same time, the noise increment at BPF frequency from small to middle propeller is 19.23 dB and 33.02 dB at 2BPF. However, the noise enhancement from the middle to big propeller is only 6.65 dB at BPF and 5.94 dB at 2BPF, which differs markedly to the conclusion of radiating equivalent sound pressure level from different scaled air-propeller measured with uniform inflow and the same relative distance in wind tunnel in Ref. [42]. One reason is the difference of incoming inflow, and the other is the scale effect of developing cavitation on noise. On this point, the difference of tonal component frequencies for three propellers is just attributed to the interactions between different cavitation level with a similar incoming flow. In detail, the predominate line spectrum of small propeller is located at BPF, while the 2BPF for the middle and both 2BPF and 3BPF for the big. Additionally, it also draws a conclusion that, with the same scale ratio and a similar observer distance, the scale effects are weakened a lot by the increase of model scale.

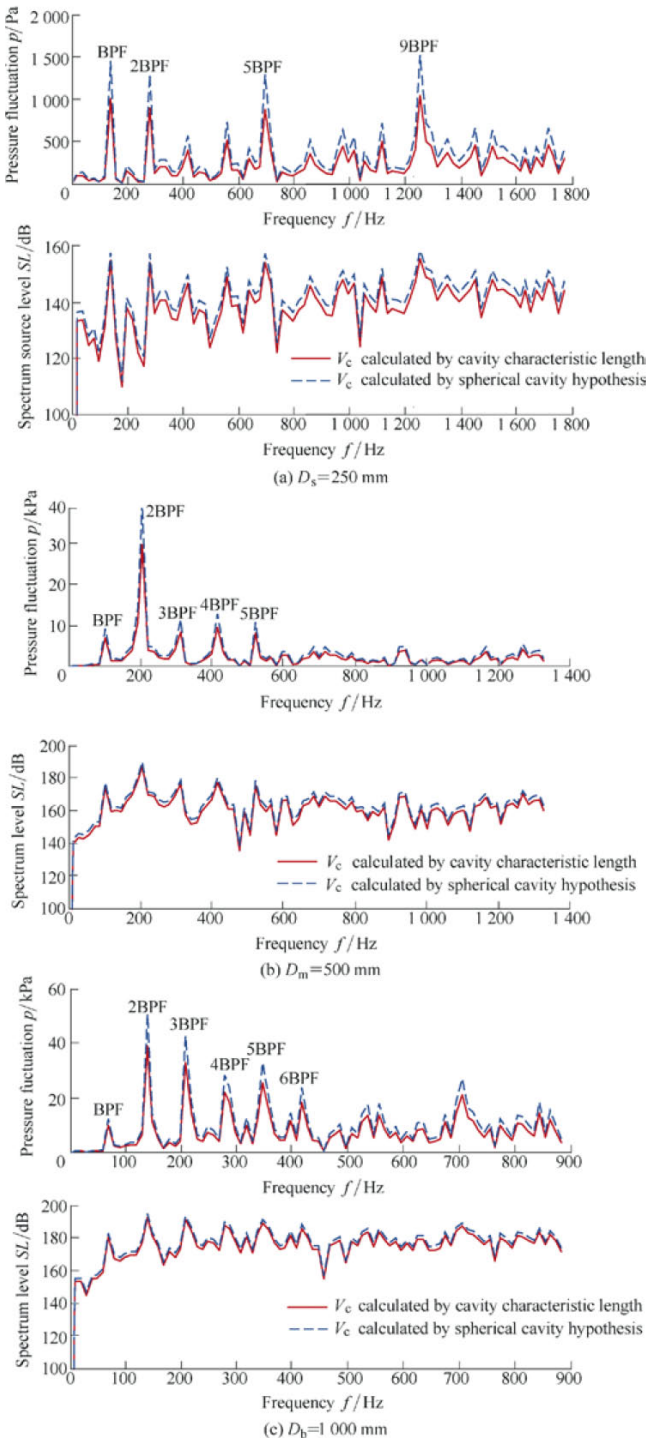

Fig. 12. Cavitating noise spectrum at low frequency of propellers under condition of $J_p = 0.403, \sigma = 2.5$

Fig. 13 shows the non-dimensional cavitating noise

spectrum of all scales under the same condition as that in Fig. 12. It is found that the spectrum level of big propeller is about 6 dB higher than that of the middle at the first two line spectrum frequencies and over 10 dB above the 3BPF harmonics. At the same time, the increments exceeding 20 dB is found from small to middle propeller. It is inferred that, with a same scale ratio, the effects of interactions between non-uniform inflow with pulsating cavity volume on cavitating line spectrum will be enlarged aligned with a smaller model scale, and more scale effects will be presented subsequently, seen in Fig. 14 for comparisons of the line spectrums of three propellers, which is consistent with the analysis above.

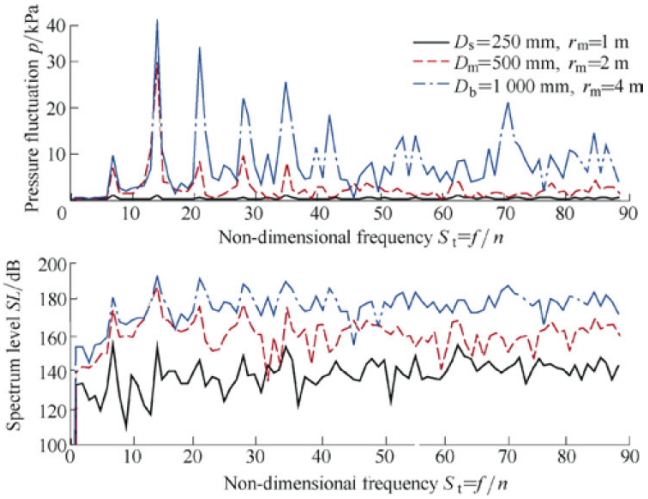

Fig. 13. Comparison of cavitation noise spectrum of propellers under condition of $J_p = 0.403, \sigma = 2.5$

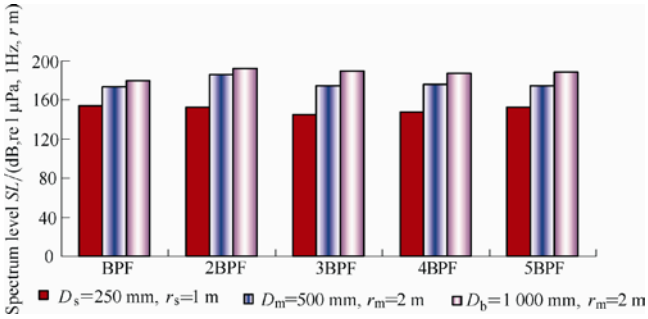

Fig. 14. Comparison of cavitating line spectrum of propellers under condition of $J_p = 0.403, \sigma = 2.5$

In the light of the engineering application, the increase in noise scaling from model to full scale recommended by ITTC is given by

$$\Delta SL = 20\lg\left(\left(\frac{D_{pro}}{D_{mod}}\right)^z\left(\frac{r_{mod}}{r_{pro}}\right)^x\left(\frac{\sigma_{npro}}{\sigma_{nmod}}\right)^{y/2}\left(\frac{n_{pro}D_{pro}}{n_{mod}D_{mod}}\right)^y\left(\frac{\rho_{pro}}{\rho_{mod}}\right)^{y/2}\right), \tag{17}$$

where ΔSL is the increase of spectrum level, subscripts pro and mod refer to the full scale and model respectively. Referring to ATLAR, at al[3], the power value is $x = 1, y = 2, z = 1$. The frequency shifts with

$$\frac{f_{pro}}{f_{mod}} = \frac{n_{pro}}{n_{mod}}. \tag{18}$$

In Ref. [3], the diameter of model propeller is 300 mm, which is a litter bigger than the small propeller in this research. When the same cavitation number between full and model scale as well as a similar reference distance is considered, the expression for the increase in noise level reduces to

$$\Delta SL = 20\lg\left(\lambda^2\left(\frac{n_{pro}}{n_{mod}}\right)^2\right), \tag{19}$$

in which $\lambda = D_{pro}/D_{mod}$ is the scale ratio. Applying this equation, there should be a 7.04 dB incensement of the spectrum level at a certain frequency from small to middle propeller, and 5.00 dB increment from middle to the big propeller at the same time. Relating to the predicted about 6 dB increase from middle to big propeller, it is seen that the scaling law is roughly appropriate when the middle propeller is chose as model. In this case, the difference between the predicted spectrum level of big propeller by the hybrid method and by the scaling law is in the same order of magnitude to the measurement precision in Ref. [3], which can be just to demonstrate the credibility of the used numerical hybrid method.

5 Conclusions

(1) With the same cavitation number, the propeller thrust coefficient increases but torque coefficient decreases with geometrical scale. And the beginning point of thrust decline induced by cavitation is moved forwards with diameter increase but followed a comparable rate of cutoff after the point. The calculated power value of local Reynolds number represented the scale effect on cavitation inception number is 0.11.

(2) In conjunction with the pulsating spherical bubble radiated noise theory based on characteristic length of sheet cavitation, the multi-phase flow cavitation simulations predict the leading line spectrum of small propeller is located at BPF, while 2BPF for the middle propeller and both 2BPF and 3BPF for the big propeller, which shows a close relationship between the cavitating tonal components with the interaction between non-uniform inflow and the pulsating cavity volume.

(3) The numerically predicted increment of noise spectrum level from middle to big propeller is 6.65 dB at BPF and 5.94 dB at 2BPF, which just differs less than 2 dB to the values obtained by scaling law recommended by ITTC. It means if the middle propeller is used as model, the scaling law is roughly suitable in engineering. And note that its error is enlarged sharply with a smaller model scale

especially to the cavitating tonal noise components.

References

[1] KELLER A P. Cavitation scale effects empirically found relations and the correlation of cavitation number and hydrodynamic coefficients[C]// *Proceedings of the Fourth International Symposium on Cavitation*, Pasadena, 2001, lecture 001: 1–18.

[2] SZANTYR J A. Scale effects in cavitaion experiments with marine propeller models[J]. *Polish Maritime Research*, 2006, 4: 3–10.

[3] ATLAR M, TAKINACI A C, KORKUT E. Cavitation tunnel tests for propeller noise of a FRV and comparisons with full-scale measurements[C]// *Proceedings of the Fourth International Symposium on Cavitation*, Pasadena, 2001, session B8. 007: 1–14.

[4] SHEN Y T, STRASBERG M. *The effect of scale on propeller tip-vortex cavitation noise*[R]. USA: Naval Surface Warfare Center Report, NSWCCD-50-TR-2003/057, 2003.

[5] HSIAO C T, CHAHINE G L. Scaling of tip vortex cavitation inception noise with a bubble dynamics model accounting for nuclei size distribution[J]. *ASME Journal of Fluids Engineering*, 2005, 127: 55–65.

[6] HSIAO C T, CHAHINE G L. Scaling of tip vortex cavitation inception for a marine open propeller[C]// *27th Symposium on Naval Hydrodynamics,* Seoul, Korea, October 5-10, 2008: 1–10.

[7] PARK K, SEOL H, CHOI W, et al. Numerical prediction of tip vortex cavitation behavior and noise considering nuclei size and distribution[J]. *Applied Acoustics*, 2009, 70: 674–680.

[8] SINGHAL A K, ATHAVALE M M, LI Huiying, et al. Mathematical basis and validation of the full cavitation model[J]. *ASME Journal of Fluids Engineering,* 2002, 124(4): 617–624.

[9] GINDROZ B, BILLET M L. Nuclei and acoustic cavitation inception of ship propellers[C]// *Proceedings of 2nd International Symposium on Cavitation*, Tokyo, Japan, 1994.

[10] KORKUT E, ATLAR M. On the important of the effect of turbulence in cavitation inception tests of marine propellers[J]. *Proc. R. Soc. Lond.* A, 2012, 458: 29–48.

[11] SALVATORE F, TESTA C, GRECO L. Coupled hydrodynamics-hydroacoustics BEM modeling of marine propellers operating in a wakefield[C]// *Proceedings of the First International Symposium on Marine Propulsors*, Trondheim, Norway, Juen, 2009, WB1-3: 1–11.

[12] EKINCI S, CELIK F, GUNER M. A practical noise prediction method for cavitating marine propellers[J]. *Brodogradnja*, 2010, 61(4): 359–366. DOI: http://hrcak.srce.hr/file/94695.

[13] SEOL H, CHEOLSOO P. Numerical and experimental study on the marine propeller noise[C]//*19th International Congress on Acoustics,* Madrid, September 2–7, 2007: 1–4.

[14] HU Jiang. *Research on propeller cavitation characteristics and low noise propeller design*[D]. Harbin: Harbin Engineering University, 2006. (in Chinese)

[15] ZHANG Yongkun. *Investigation on predicting ship propeller radiated noise*[D]. Wuhan: Naval University of Engineering, 2009. (in Chinese)

[16] TESTA C. *Acoustic formulations for aeronautical and naval rotorcraft noise prediction based on the Ffowcs Willians and Hawkings equation*[D]. Netherlands: Delft University of Technology, 2008.

[17] SAUER J. *Instationaren kaviterende stromung — ein neues model, baserend auf front capturing (VOF) and blasendynamik*[D]. Karlsruhe: Universitat Karlsruhe, 2000.

[18] KUNZ R F, BOGER D A, STINEBRING D R, et al. A preconditioned Navier-Stokes method for two-phase flows with application to cavitation prediction[J]. *Computers & Fluids*, 2000, 29(8): 849–875.

[19] ZWART P J, GERBER A G, BELAMRI T. A two-phase flow model for predicting cavitation dynamics[C]// *Proceedings of 5th International Conference on Multiphase Flow*, Yokohama, Japan, 2004.

[20] RHEE S H, KAWAMURA T, LI Huiying. Propeller cavitation study using an unstructured grid based Navier-Stokes solver[J]. *ASME Journal of Fluids Engineering*, 2005, 127(5): 986–994.

[21] LINDAU J W, MOODY W L, KINZEL M P, et al. Computation of cavitating flow through marine propulsors[C]// *Proceedings of First International Symposium on Marine Propulsors*, Trondheim, Norway, Juen, 2009, MB3-2: 1–10.

[22] KIM S E. Multiphase CFD simulation of turbulent cavitating flows in and around marine propulsors[C]// *Proceedings of Open Source CFD International Conference 2009*, Barcelona, Spain, 2009.

[23] OLSSON M. *Numerical investigation on the cavitating flow in a waterjet pump*[D]. Sweden: Chalmers University of Technology, 2008.

[24] MORGUT M, NOBILE E. Influence of the mass transfer model on the numerical prediction of the cavitating flow around a marine propeller[C]// *Proceedings of Second International Symposium on Marine Propulsors*, Hamburg, Germany, 2011:1–8.

[25] JI Bin, LUO Xianwu, WANG Xin, et al. Unsteady numerical simulation of cavitating turbulent flow around a highly skewed model marine propeller[J]. *ASME Journal of Fluids Engineering*, 2011, 133, 011102: 1–8.

[26] YANG Qiongfang, WANG Yongsheng, ZHANG Zhihong. Assessment of the improved cavitation model and modified turbulence model for ship propeller cavitation simulation[J]. *Journal of Mechanical Engineering*, 2012, 48(4): 178–185. (in Chinese)

[27] YANG Qiongfang, WANG Yongsheng, ZHANG Zhihong. Determination of propeller cavitation initial inception and numerical analysis of the inception bucket[J]. *Journal of Shanghai Jiaotong University*, 2012, 46(3): 410–416. (in Chinese)

[28] YANG Qiongfang, WANG Yongsheng, ZHANG Zhihong. Multi-phase numerical simulation of propeller turbulent cavitation inception flow[J]. *Journal of Shanghai Jiaotong University*, 2012, 46(8): 1 254–1 262. (in Chinese)

[29] YANG Qiongfang, WANG Yongsheng, ZHANG Minming. Propeller cavitation viscous simulation and low frequency noise prediction with non-uniform inflow[J]. *Acta Acustica*, 2012, 37(6): 583–594. (in Chinese)

[30] YANG Qiongfang, WANG Yongsheng, ZHANG Zhihong. Improvement and evaluation of numerical model for viscous simulation of cavitating flow around propeller blade section[J]. *Transactions of Beijing Institute of Technology*, 2011, 31(12): 1 401–1 407. (in Chinese)

[31] YANG Qiongfang, WANG Yongsheng, ZHANG Zhihong. Multiphase flow simulation of propeller cavitation breakdown performance maps[J]. *J. Huazhong Univ. of Sci. & Tech. (Natural Science Edition)*, 2012, 40(2): 18–22.

[32] SHIN K W. *Cavitation simulation on marine propellers*[D]. Denmark: Technical University of Denmark, 2010.

[33] ROSS D. *Mechanics of underwater noise*[M]. New York: Pergamon Press, 1976, pp: 253–272.

[34] SEOL H, JUNG B, SUH J C, et al. Prediction of non-cavitation underwater propeller noise[J]. *Journal of Sound and Vibration*, 2002, 257(1): 131–156.

[35] FARASSAT F, SUCCI G P. The prediction of helicopter rotor discrete frequency noise[J]. *Vertica,* 1983, 7(4): 309–320.

[36] CARLEY M. *Time domain calculation of noise generated by a propeller in a flow*[D]. Ireland: Department of Mechanical Engineering in Trinity College, 1996.

[37] PEREIAR F, AVELLAN F, DUPONT P. Prediction of cavitation erosion: an energy approach[J]. *Journal of Engineering*, 1998, 120(4): 719–727.

[38] PEREIRA F, SALVATORE F, FELICE F D, et al. Experimental and numerical investigation of the cavitation pattern on a marine

propeller[C]// *24th Symposium on Naval Hydrodynamics*, office of Naval Research, Fukuoka, Japan, 2002.

[39] PEREIRA F, SALVATORE F, FELICE F D. Measurement and modeling of propeller cavitation in uniform inflow[J]. *ASME Journal of Fluids Engineering*, 2004, 126: 671–679.

[40] YANG Qiongfang, GUO Wei, WANG Yongsheng, et al. Procedural realization of pre-operation in CFD prediction of propeller hydrodynamics[J]. *Journal of Ship Mechanics*, 2012, 16(4): 375–382. (in Chinese)

[41] HAN Baoyu. *Numerical simulation of sheet cavitation and tip vortex cavitation and investigation to scale effect of tip vortex cavitation inception*[D]. Wuhan: Naval University of Engineering, 2011. (in Chinese)

[42] GAO Yongwei. *Propeller noise characteristics research by wind tunnel tests and numerical simulation*[D]. Xian: Northwestern Polytechnical University, 2004. (in Chinese)

Biographical notes

YANG Qiongfang, born in 1984, is currently a lecturer and a young hydrodynamicist at *Office of Marine Propulsion New Technologies in College of Marine Power Engineering, Naval University of Engineering, China*. He received his PhD degree in marine engineering in 2011. He has been responsible for the hydrodynamics and hydroacoustics prediction of ship and submarine's propulsors under non-cavitation and cavitation conditions, including open controllable pitch propeller, contra-rotating propeller, waterjet and pumpjet. His especial research interests are located at low noise propulsors design, including delaying the cavitation inception of the waterjet and pumpjet after numerical determination of the critical point, and controlling their directly radiated noise.
Tel: +86-27-83443595; E-mail: yqfhaijun2008@126.com

WANG Yongsheng, born in 1955, is currently a professor and a PhD candidate supervisor at *Naval University of Engineering, China*. He received his PhD degree from *Huazhong Universtiy of Technology, China*, in 2002. His research interests include simulation of static & dynamic performances of marine power plant, ship waterjet technology, and ship radiated noise prediction.
Tel: +86-27-83444642; E-mail: yongshengwang666@126.com

ZHANG Zhihong, born in 1964, is currently a professor, a PhD candidate supervisor and a Senior Specialist in fluids mechanics at *College of Science, Naval University of Engineering, China*. His main research interests include super-cavitation, cavitation multiphase flow and CFD.
Tel: +86-27-83444975; E-mail: zhangzhihong_999@163.com